Applied Physics A (2023) 129:13
https://doi.org/10.1007/s00339-022-06279-1

Applied Physics A
Materials Science & Processing

Bambusa arundinacea leaves extract-derived Ag NPs: evaluation of the photocatalytic, antioxidant, antibacterial, and anticancer activities

N. Jayarambabu[1] · Suresh Velupla[2] · A. Akshaykranth[1] · N. Anitha[1] · T. Venkatappa Rao[1]

Received: 11 August 2022 / Accepted: 25 November 2022 / Published online: 7 December 2022

Abstract
Bio-fabrication has become a safe approach for silver nanoparticles (Ag NPs). The plant-mediated biosynthesized Ag NPs have emerged as a potential substitute for conventional chemical formation. The biosynthesized Ag NPs were analyzed in terms of crystalline nature, morphology, chemical composition, particle size, stability, size, and shape of the particles. The XRD, FTIR, and TEM analysis indicate the presence of the bioactive secondary metabolites compounds. The bamboo-mediated Ag NPs demonstrated a notable antibacterial efficacy against Gram-positive and Gram-negative pathogenic microorganisms and showed significant antioxidant activity against DPPH free radicals. The degradation of methylene blue at various intervals under solar light irradiation was used to evaluate the photocatalytic performance of Ag NPs. Further, Ag NPs conveyed potent anticancer activity against MCF-7 cell lines with a significant value IC_{50}. The bamboo leaves-mediated Ag NPs synthesized Ag NPs signified strong antibacterial, antioxidant, and anticancer activity; hence, it can be used in various biomedical applications and face mask coating to prevent the coronavirus after successful clinical trials in research laboratories.

Keywords Antioxidant · Antibacterial · Anticancer activity · Ag nanoparticles · Bambusa arundinacea · Photocatalytic activity

1 Introduction

Nanotechnology is a rapidly evolving multidiscipline that contains designing, synthesizing, assembling, and modifying molecules/ bulk matter/ particles to nanostructured dimensions (1–100 nm in size) [1]. Nanoparticles have a large surface-to-volume ratio, giving them unique features and improving their mechanical, catalytic, optical, and magnetic properties, allowing them to be used in biomedical applications. They have been widely employed in medical, food, agriculture, optics, the environment, mechanics, chemical, photochemical, catalysis, cosmetics, electronics, sensing technologies, energy research, and other fields [2]. There are two types of nanoparticles: inorganic and organic. Metallic (Au, Ag), semiconductor (CdS, ZnO), and magnetic (Ni, Co) nanoparticles are the most common inorganic nanoparticles, whereas organic nanoparticles are carbon-based nanoparticles (carbon nanotubes, quantum dots) [3]. Metallic nanoparticles, in particular, have been widely exploited for various applications due to their unique features. Metallic nanoparticles' therapeutic efficacy is owing to their optical property, which is proved by localized surface plasmon resonance [4]. Silver nanoparticles (Ag Nps) are particularly common among metal nanoparticles. They have many applications in biomedicine and industry due to nanoparticles' physical, thermal, optical, chemical, catalytic activity, electrical conductivity, and antibacterial activity. These unique qualities have allowed Ag NPs to be used in various sectors such as antifungal, antiviral, anticancer, anti-inflammatory, drug administration, sensing, diagnostics, orthopedics, and so on [5].

The efficiency of Ag NPs inside biological systems is influenced by the size, surface chemistry, shape, size distribution, particle morphology, coating agglomeration,

✉ T. Venkatappa Rao
tvraokmm@nitw.ac.in

[1] Department of Physics, National Institute of Technology, Warangal 506004, India

[2] Department of Biochemistry, Osmania University, Hyderabad 500007, India

dissolving rate, and particle composition [6]. Silver is a non-toxic, harmless inorganic antibacterial agent that can kill over 650 different species of disease-causing bacteria [7, 8]. Various methods have been devised for the preparation of nanoparticles, each with its own set of benefits and drawbacks [9]. Metallic nanoparticles can be made using both chemical and physical processes. Although these technologies create particles with the desired properties, they are frequently expensive, time consuming, and undesirably harmful to living creatures and the environment. The biological technique has been utilized to generate nanoparticles to overcome the limitations of these physical and chemical technologies. Several biological resources have been employed to produce metal nanoparticles, including plant extracts, milk, microbes, and panchagavya [10, 11]. Among the different green sources investigated, microalgae offer essential advantages in terms of ease of development and living in harsh settings (such as temperature and pH) [12]. Recently, numerous advantages of biological Ag NPs production have been recognized. Several plant materials and microorganisms have been identified as possible Ag NPs production candidates. Specific proteins in plants and microorganisms have been postulated as a possible source of Ag^+ ion reduction. It has been postulated that NADH-dependent nitrate reductase may reduce Ag^+ ions to Ag^0 ions [13]. However, the synthesis of Ag NPs using plant extracts has the potential to be more advantageous than microbes due to its simplicity in scaling up. [14]. Using microorganisms has some drawbacks, including high costs, aseptic environment upkeep, mass microbe cultivation, output quantity, and purification [13]. On the other hand, the green method involves using plant extracts, is environmentally friendly, cost-effective, and efficient [15]. Several researchers employing plant extracts such as Carica papaya [16], Azadirachta indica [17], Alternanthera dentata [18], Olea europaea [19], and Coffea Arabica [20] have been conducted in recent years to synthesize nanoparticles. Furthermore, plant extracts from various species are regarded as a beneficial approach for nanoparticle synthesis due to their extraordinary ability to synthesize a wide range of phytochemicals with a high reduction potential [19]. Sugars, polyphenols, terpenoids, alkaloids, proteins, and phenolic acids reduce metal ions into nanoparticles. These phytochemicals are also responsible for stabilizing the nanoparticles produced [21]. All parts of the bamboo plant, including the rhizome, bark, culm, leaves, shoots, roots, and seeds, have been used in clinical and therapeutic. Bamboo is the fastest-growing multipurpose woody plant. The natural substances abundant in bamboo leaves, including phenols, flavonoids, saponins, vitamins, glycosides, antioxidants, and some other compounds, have a role in reducing silver nitrate to Ag NPs (Table 1). At the same time, these compounds bound on the surface of the Ag NPs and enhanced the biological activities due to the presence of biological compounds.

Table 1 Bioactive compounds of Bambusa arundinacea

Phytochemical compound	Reference
Alkaloids	[22]
Carbohydrates	[23]
Glycosides	[24]
Saponins	[25]
Phytosterol	[26]
Resins	
Phenols	
Fixed oil	
Tannins	
Diterpenes	
Protein and amino acid	
Flavonoids	
Alkaloids	
Carbohydrates	
Glycosides	
Saponins	

In this present study, Ag NPs were green synthesized by the reduction of silver precursor in the presence of plant extract sources. The benefits of green synthesis techniques, ease of nanoparticle creation, eco-friendly, cost effectiveness, quick crystallization, and reduced waste generation are all demonstrated by the plant extract sources employed for the bio-reduction of silver nitrate to Ag NPs. The synthesized Ag NPs were analyzed by X-ray diffraction (XRD), FTIR spectroscopy, scanning electron microscopy (SEM), UV–Visible spectroscopy, dynamic light scattering (DLS), and TEM to investigates the antibacterial, antioxidant, anticancer, and photocatalytic activities of Ag NPs'.

2 Materials and methods

2.1 Materials

Bambusa arundinacea leaves' extract solution, silver nitrate (Sigma Aldrich) 2, 2-diphenyl-1-picrylhydrazyle (DPPH) were purchased from Sigma-Aldrich, St. Louis, MO, USA.

2.2 Preparation of the plant extract

An extract of the Bambusa arundinacea leaves was used for the biogenic synthesis of Ag NPs. The leaves have been used as medicine for various inflammatory conditions. The leaves were washed with double distilled water to remove the dust and mud particles on the leaves' surface, and these were finely cut into small pieces before going to dry in the

presence of sunlight. 20 gm of the leaves was immersed into 100 ml double distilled water and placed on the magnetic stirrer for 70 min at 80 °C to prepare for extractions of the solution. A Whatman filter paper used for filtration of the extract solution was kept at room temperature for cooling and finally used for the biogenic synthesis of Ag NPs.

2.3 Biogenic synthesis of Ag NPs

For the biogenic synthesis of Ag NPs, 0.5 mM silver nitrate was prepared in 100 mL double distilled water. The aqueous solution of the leaves' extract was added to the above solution and stirred for 4 h at a temperature of up to 60 °C. Under these circumstances, the solution's color changed from a colorless solution to dark color due to the Ag^{+} conversion into Ag^{o} ions. Bamboo leaves extract as a reduction agent for the synthesis of Ag nanoparticles. Bamboo leaves contain phytoconstituents which help to stabilize the Ag nanoparticles as shown in Fig. 1. The biogenic synthesized Ag NPs were characterized with different analytic techniques for their morphology, stability, chemical compositions, crystallinity, and particle size.

2.4 Antibacterial activity

The antibacterial activity of Ag NPs was investigated using the suitable disc diffusion method. The bacteria were isolated from an initial single colony and were grown overnight in nutrient broth. The items, including the glassware, reagents, and medium, were sterilized in an autoclave at 121 °C for 20 min under 15 kg/cm^2 pressure. The bacterial inoculum was incubated in lysogeny broth for 24 h at 28 °C and 200 rpm, then re-suspended in a lysogeny broth medium until the optical density was adjusted to 0.1 at 600 nm, which corresponds to 10^8 colony-forming units (CFU)/mL. The spread plate method was performed in this bacterial suspension (each 100 µl) spread on the nutrient agar. Subsequently, wells were made on agar plates, and various concentrations of Ag were loaded. The entire agar plates were placed in the bacteriological incubator for 24 h at 37 °C, and the zone of inhibition was calculated with a measuring scale (mm).

2.5 DPPH scavenging assay

Ag NPs were investigated by DPPH (1, 1-diphenyl-2-picrylhydrazyle) scavenging assay. To the DPPH (50 µM) solution prepared in absolute ethanol (in the dark), various concentrations were added to 96-well microtitre plates. After adding NPs, the plate was placed in the dark, and the reaction samples were incubated for 30–60 min at room temperature. The DPPH solution incubated with reference standard ascorbic acid (25 µg/mL) and bamboo leaves extract served as positive and negative controls, respectively. The AgNPs sample was evaluated in triplicates, and the absorbance was recorded at 520 nm using a microplate reader (Micro Scan, MS5608A, ECIL, and India). A decrease in absorbance was recorded for calculating DPPH scavenging (%) using the following equation [27].

$$\text{DPPH scavenging activity (\%)} = \frac{\text{DPPH absorbance} - \text{sample absorbance}}{\text{DPPH absorbance}} \times 100$$

2.6 MTT assay

To test the cell viability (MTT) assay, the breast cancer cell line (MCF-7) was collected from the National Centre for Cell Sciences India. The cells were grown in Dulbecco's modified Eagles medium (DMEM) containing 10% fetal bovine serum (FBS), 100 units/mL penicillin G and 1 µg/ streptomycin, 5 µg/mL amphotericin B (Sigma-Aldrich Chemicals, St. Louis, United States) (2 mM) L-glutamine and non-essential amino acids (1X), (Himedia, Mumbai, India) at 37 °C in a humidified 5% CO_2 incubator Nectarnova, Symbiogen, Chennai, India). Cytotoxicity of the nanoparticles was studied under the conditions after 80% confluence. Cells were trypsinized with 0.1% trypsin–EDTA and

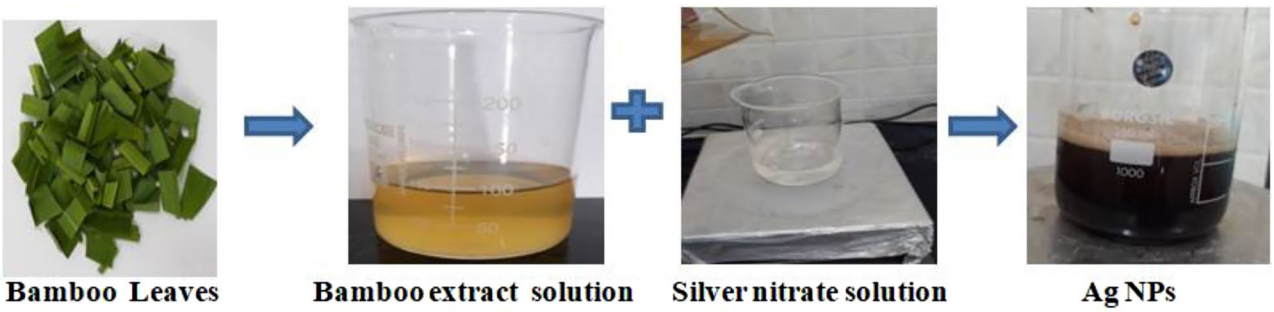

Fig. 1 Biogenic synthesis of Ag NPs

were harvested by centrifugation at 500 × g. Serial dilutions of cells were made from 1×10^6 to 1×10^3 cells per mL.

The cells were seeded in triplicates in a 96-well plate. The suspended cells were treated with 20, 40, 60, 80, and 100 µL concentrations of AgNPs, in a dose-dependent way for 24 h. Tamoxifen drug was used as a positive control, and tumor cells without nanoparticles were added to serve as a control. After incubation, MTT (20 µl, 5 mg/mL) solution was added to each well, and the cell viability was calculated by measuring the ability of cells to transform MTT to a purple-colored formazan dye. At 570 nm, the absorbance was observed using an ELISA instrument (MS5608A from ECIL, Hyderabad, India). The percent cell viability was measured using the following equation [28]

$$\text{Percent cell viability} = \frac{A570\text{sample}}{A570\text{control}} X100$$

where A 570 (sample) corresponds to absorbance obtained from the wells treated with nanoparticles, and A 570 (control) represents the absorbance from the wells in which no nanoparticle construct was added.

3 Characterization of Ag nanoparticles

The following analytical techniques carried out the characterizations of biogenic synthesized Ag NPs. First, the purity and crystallinity of Ag NPs were observed by powder XRD (Bruker advanced D8). The functional groups of biogenic nanoparticles were identified by FTIR, ranging from 500 to 4000 cm-1 (Bruker Alpha-II). The particle size and stability of the nanoparticles were measured by dynamic light scattering (DLS) (Horiba-SZ100). UV–Vis analysis was performed by spectrophotometer between 200 to 800 nm (Analytical Jena, Specord 210 Plus). The morphology of the biogenic synthesized sample was analyzed by field emission scanning microscope (FESEM, Carl Zeiss, Ultra Plus) size and shape of the nanoparticles were analyzed by TEM. Finally, X-ray photoelectron spectroscopy XPS (PHI 5600 Versa Probe III) was used to analyze the synthesized samples' surface components.

4 Results and discussion

Biosynthesized Ag NPs indicated the five diffraction peaks at 2θ position 32.20°, 38.16°, 46.15°, 67.40°, and 76.10°. These peaks correspond to the (122), (111), (200), (220), and (311) planes, respectively, and showed the face-centered cubic structure as shown in Fig. 2a. The unwanted peaks in the spectrum indicated the presence of various bioactive reducing agents and capping compounds accumulated on the surface of Ag NPs. The reducing agents of plant extract compounds were responsible for the synthesis of Ag NPs [29].

UV–Visible spectroscopy is the primary tool to confirm that as-synthesized materials are nanoparticles. Figure 2b shows UV analysis of as-synthesized Ag NPs mediated by Bambusa arundinacea leaves extract. The range of absorption spectra was between 200 to 800 nm, and the peak position appeared at 452 nm, indicating the formation of Ag NPs. The plasmon resonances of Ag were observed near 452 nm [30]. The metal contains the free electrons that go through plasmon resonance transitions in the visible spectrum, which gives rise to such strong colors. This type of property mostly appeared in Ag NPs due to the occurrence of free conduction electrons. The electric field of the inward radiation induces the creation of a dipole in the nanoparticles. The number of factors depends on the wavelength of oscillation. The nature of medium particles' size, as well as shape, were the most important ones.

FTIR analysis of the Ag NPs prepared from Bambusa arundinacea leaves extract is shown in Fig. 2c. The characteristic peaks around 3434 cm^{-1} were ascribed to the OH stretching vibration of the OH structure. The peaks around 2937 and 2368 cm^{-1}were ascribed to C–H stretching vibrations. The peak position at 1611 cm-1 was ascribed to the C = C stretching vibration of aromatic rings. The peak at 1380 cm^{-1} was assigned to polyphenols group compounds [31–33].

Additionally, the peak around 1016 was attributed to alkynes C–H bending vibration. The peak position at 573 and 450 cm^{-1}indicated the Ag NPs. The FTIR results verified that the bioactive compounds in the aqueous were distributed on the surface of Ag NPs and also responsible for the reduction and capping agent of silver ions, which is consistence with the previous reports.

The FESEM analysis was determined to evaluate the morphology, shape, size, and uniformity of the distribution of the Ag NPs. Figure 3a, b shows the FESEM images of biosynthesized Ag NPsat scales of 100 and 200 nm. Based on the FESEM images, the spherical nature of the Ag NPs was found [34]. The FESEM images showed that the average particle diameter of the synthesized Ag NPs varied in the range of 20–50 nm. The TEM analysis was determined to accurately investigate the shape and size of the synthesized Ag NPs. In the TEM images, the sizes of the nanoparticles were in the range of 30–40 nm with spherical structure particles [35]. In addition, the TEM analysis revealed the bioactive compounds' presence on the surface of the Ag NPs in Fig. 3d, e.

The average particle size of the biosynthesized Ag NPs was measured by dynamic light scattering (DLS) measurement. The DLS analysis showed that Ag NPs had an average particle size of 23.6 nm in Fig. 3f. In addition, the zeta

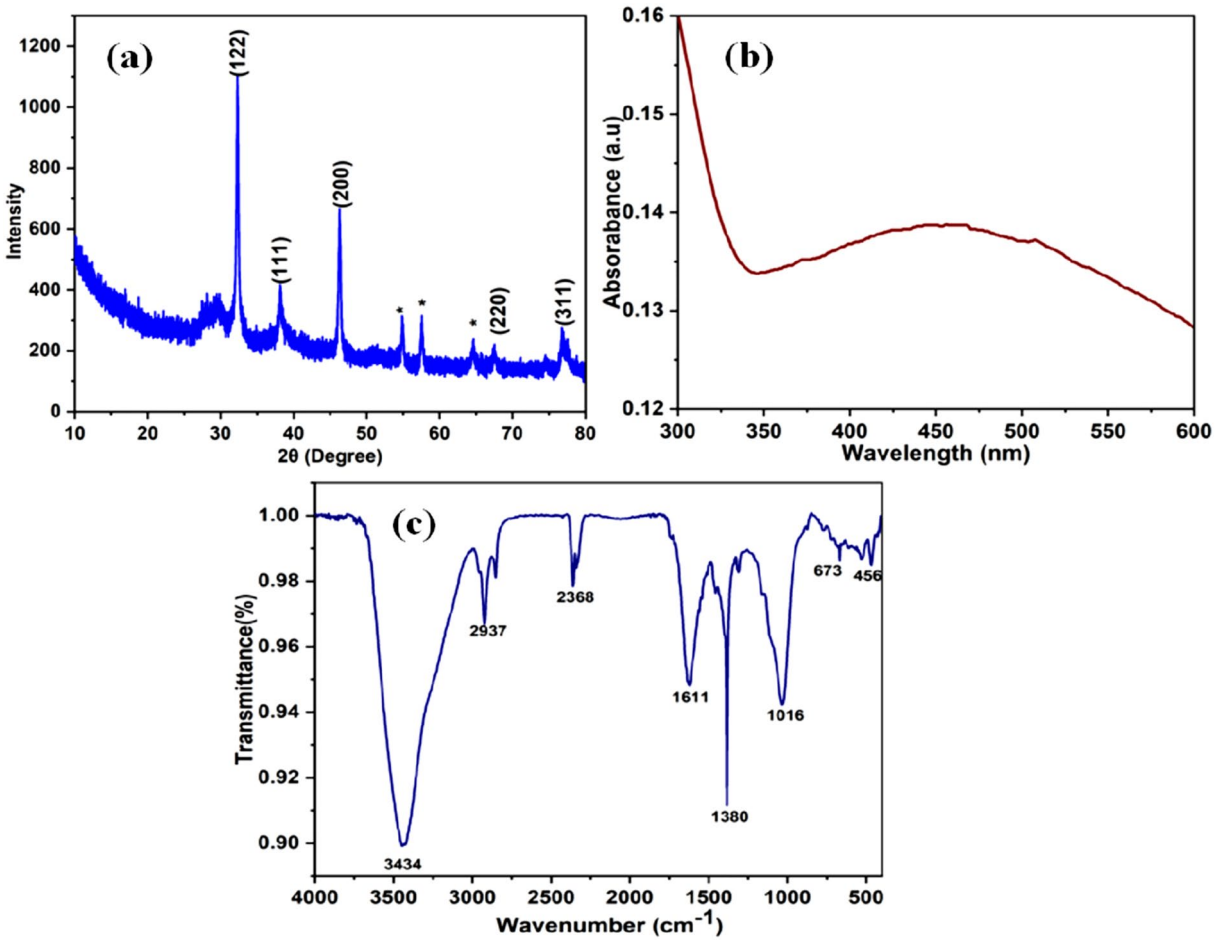

Fig. 2 **a** X-ray diffraction pattern **b** UV–Visible spectra **c** FTIR spectra of biogenic synthesized Ag NPs

potentials analyzer was observed to identify the stability of the Ag NPs and found to be − 19.3 mV as shown in Fig. 3c. The negative value of the zeta potential indicates that the components such as phenolic, flavonoids, glycosides, saponins, tennis, antioxidants, etc., present in the leaves extract solutions act as capping agents and stabilize the Ag NPs. Hence, the sufficient charge on the surface of NPs which is compatible with the repulsive force will stop the NPs agglomeration.

4.1 XPS analysis

The chemical state and near-surface composition of Ag NPs derived from bamboo leaves extract were confirmed by X-ray photoelectron spectroscopy. An XPS spectrum of the Ag NPs in the range of 0–800 eV is depicted in the Fig. 4a. The presence of such elements as carbon (C 1 s), silver (Ag3d), and oxygen (O 1 s) was observed. Figure 4b shows the binding energy (BE) associated with the Ag3d region of the sample utilizing high-resolution XPS (HR-XPS). Two peaks at 372 and 366 eV, produced by the orbital spin interplanetary splitting corresponding to the Ag 3d3/2 and Ag 3d5/2 core levels, are critical characteristics of the Ag3d region. The other peaks at 531 and 282 eV correspond to O1s and C1s. The O1s appearing in the region between 529–535 eV due to oxygen–carbon or water incorporated on the surface of the Ag NPs are shown in Fig. 4c. The C–C binding energy contribution at 282 eV corresponds to SP^2 (C = C) [36, 37].

4.2 Photocatalytic activity of biosynthesized Ag NPs

The degradation of azo dyes, such as methylene blue, was investigated in reactions utilizing the UV-irradiation approach to evaluate the photocatalytic activity of green synthesized Ag nanoparticles. Initial color changes caused by the catalytic breakdown of organic dyes in the presence of Ag NPs were visible. Methylene blue color intensity gradually turned from dark blue to white in UV irradiation, demonstrating the effective catalytic degrading activity of Ag NPs. This work used the radioactive dye methylene blue

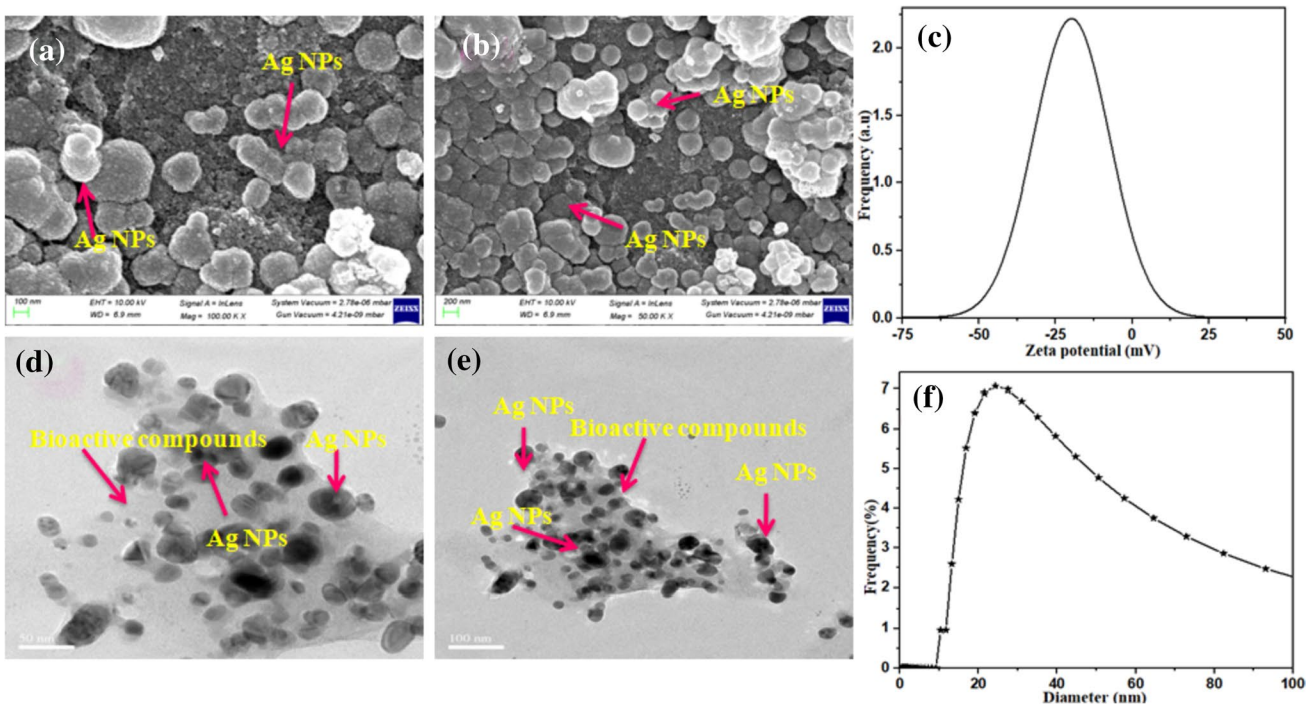

Fig. 3 **a**, **b** FESEM images **c** zeta potential **d**, **e** TEM images **f** DLS particles size of biogenic synthesized Ag NPs

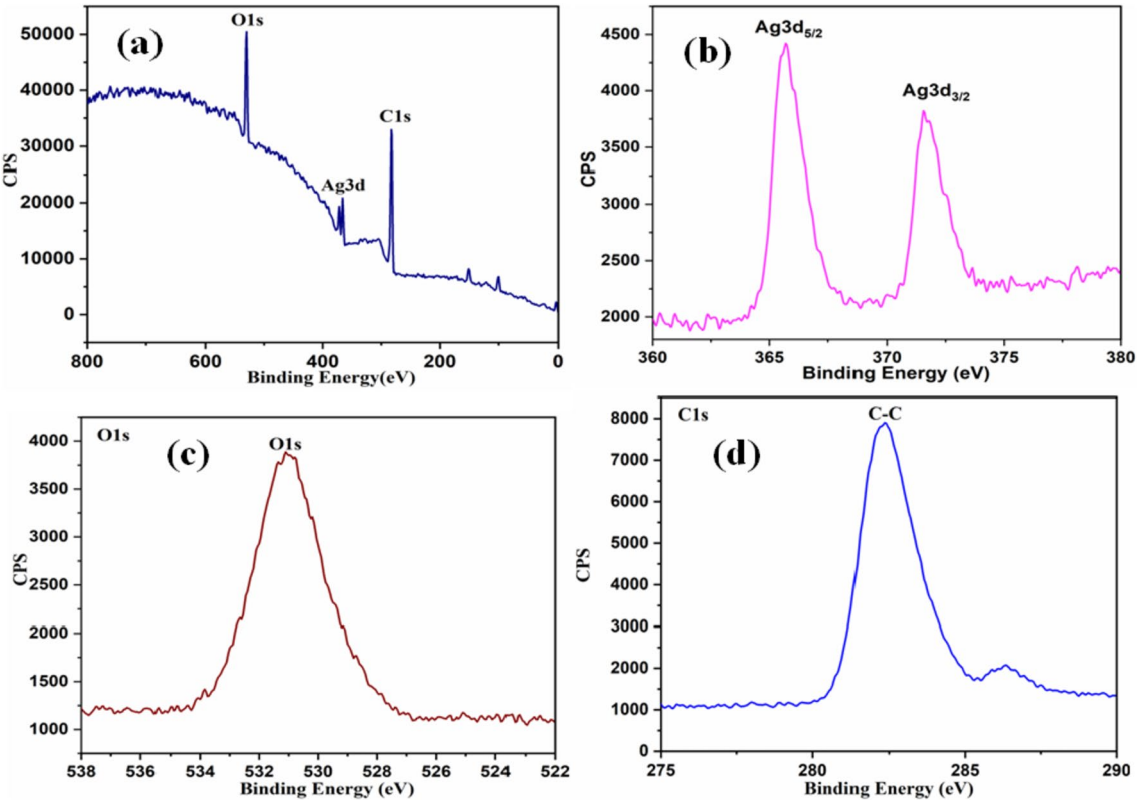

Fig. 4 XPS spectra of **a** Ag NPs XPS survey spectrum **b** binding energy for Ag3d **c** binding energy for O1s **d** binding energy for C1s

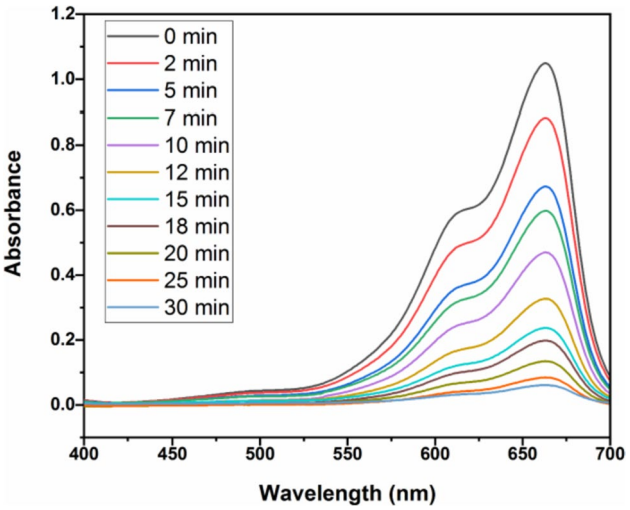

Fig. 5 Photocatalytic activity of biosynthesized Ag NPs as a nanocatalyst in the presence of $NaBH_4$

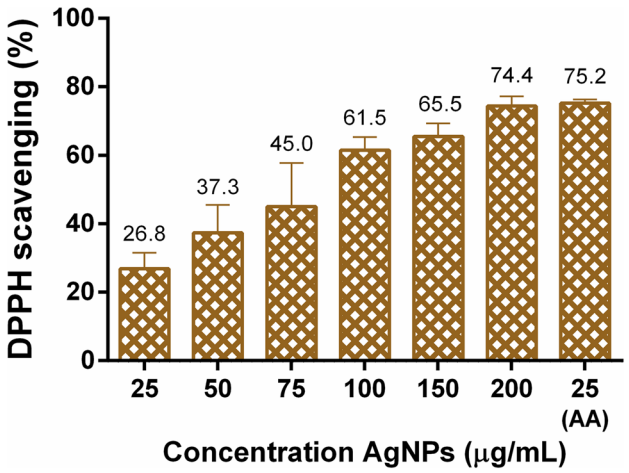

Fig. 6 Depiction of percent scavenging activity of bamboo-mediated Ag NPs with various concentrations along with positive control ascorbic acid (AA)

to test the potential nanomaterial as Ag NPs photocatalytic activity. Figure 5 shows the results; as the irradiation time increased, the efficiency of methylene blue decolorization gradually increased (up to 30 min). UV–Vis absorption spectra of MB dyes at different times showed decreasing peaks with the color shift into light color. When exposed to light, the MB absorption peak at 660 nm initially showed a rapid drop every 2 min. Ag NPs percentage of decolorization activity under UV irradiation may have reduced the amount of methylene blue (80 percent). However, as the exposure time lengthened, it persisted. The surface plasmon resonance (SPR) effect causes conduction electrons to be stimulated on the surface of silver nanoparticles when light photons interact with the Ag NPs. The surface hydroxyl groups can scavenge electron holes produced by the ultraviolet light system, which leads to the production of reactive oxygen species (ROS) and the start of the organic oxidation reaction. The size and shape of the metal nanoparticles, as well as the kind and structure of the dispersion medium, all impacted the interaction [38, 39]. As Ag NPs, a putative-reducing agent destroyed the azo dyes effectively. The results unequivocally show that Ag NPs effectively degrade hazardous pollutants in a photocatalytic manner from the textile sector.

Ag NPs showed potent DPPH scavenging activities at various concentrations. Among the concentrations tested, 25, 50, 75, 100, 150, and 200 showed the percent scavenging activities depicted in Fig. 6 as follows 26.8, 37.3, 45.0, 61.5, 65.5, and 74.4, respectively. The test of positive control ascorbic acid (AA) showed a maximum of 75.2% DPPH scavenging activity at 25 µg/mL. The bamboo plant has been used in traditional medicine in India (Ayurveda). It also has potential applications, especially in anti-stress and anti-aging [40]. In this work, we have elaborated on the effect of bamboo-based Ag NPs because of the antioxidant property of both the plant extract and Ag NPs. Surprisingly, bamboo-based Ag NPs showed higher antioxidant activity than a plant extract independently. Our results showed that the antioxidant DPPH scavenging properties of Ag NPs are maximum at 200 µg/mL with 74.4% compared with ascorbic acid (25 µg/mL), which showed 75.2% Fig. 6.[41] Similarly also reported the photochemical synthesis of Ag NPs using Pistacia khinjuk leaves extract (PKL@AgNPs). Overall, the bamboo-based Ag NPs showed much higher DPPH scavenging activity when compared with the only extract. This may lead to medicinal applications for Ag NPs concerning major oxidation-related diseases.

The in vitro results revealed that the Ag NPs exhibited enhanced inhibition of cancer cell proliferation. The MTT assay was carried out to evaluate the cytotoxic effects of plant-derived Ag NPs against MCF-7 (breast cancer cell lines) and calculated their percent cell viability. However, a significant decrease in the percent cell viability after 60 µL concentration tested is observed in Fig. 7. A complete change in the percent viability was observed in control (no nanoparticles added) and treated (with Ag NPs). Hence, IC_{50} (inhibitory concentration at 50%) was observed at 80µL of Ag NPs added to cancer cells Fig. 7.

4.3 Antibacterial activity

The antibacterial activity of Ag NPs was evaluated against five food-borne disease bacteria, i.e., two Gram-positive (*S. epidermis* and *B. subtilis*) and three Gram-negative (*P. aeruginosa, E.coli,* and *S. Shigella boydii*). The zones of inhibition (ZOI) of Ag NPs were determined at volumes of control, extract, 50 and 100 µl, individually. In treating two

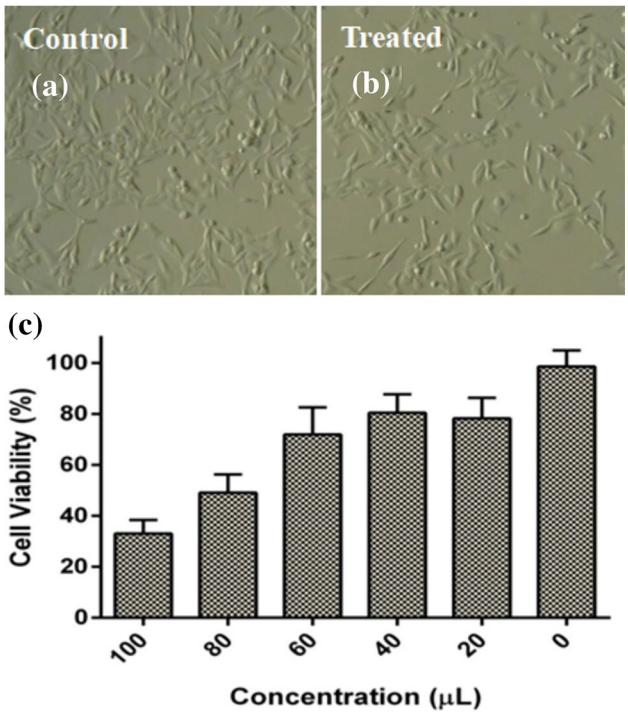

Fig. 7 MCF-7 cell lines **a** control **b** treated **c** cytotoxicity evaluation of bamboo-mediated Ag NPs at various concentrations against (MCF-7) cell lines

Gram-positive bacteria with AgNPs, the inhibition zones were observed to be 0, 4, 9, and 10 mm for *S. Epidermis* and 0, 4, 8, and 9 mm for *B. Subtilis*, and three Gram-negative bacteria (*P. aeruginosa, E.coli,* and *S. Shigella boydii*) at concentration 100 µl showed excellent activity, respectively. These results indicate Ag NPs in a concentration-dependent manner which was in concordance with the results obtained. In the present study, the maximum inhibition was seen at 100 µl of Ag NPs against *B. Subtilis* and, *S. Epidermis* and three Gram-negative at 100 µl showed excellent activity against (*P. aeruginosa, E.coli,* and *S. Shigella boydii*) as shown in Fig. 8. Some physical and chemical properties of Ag NPs were considered to elucidate their mechanism of antibacterial activity. The synthesized nanoparticles' size and shapes are critical in exerting antibacterial action. [42–44] showed that smaller-sized, spherical-shaped AgNPs displayed better germ-killing activity owing to their larger surface-to-volume ratio enabling better interaction with the bacterial cell membrane, thus destroying the respiratory system of bacteria, ultimately leading to death. This mechanism of antibacterial activity was accredited to Ag^0 ions released from metal nanoparticles which were absorbed by the bacterial cell membrane resulting in subsequent alteration in permeability of the membrane, solidification of protein structure, inhibition of respiration, and altered enzyme function, finally leading to cell membrane damage. Especially, Ag NPs, due to their elevated tendency to react with sulfur and phosphorous of biomolecules in the bacterial cell, interact and inhibit DNA replication and also destabilize and degrade the outer membrane of the plasma membrane, thus reducing the intracellular ATP. In addition, due to the presence of a single peptidoglycan layer, Gram-positive bacteria are more susceptible to the treatment of AgNPs compared to

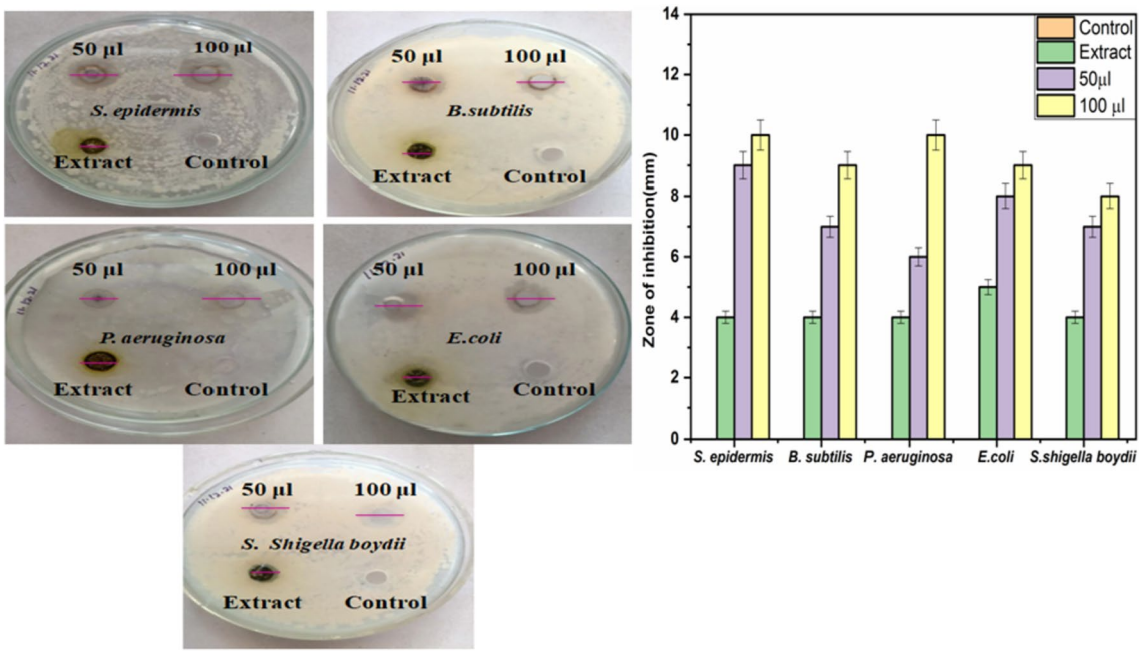

Fig. 8 Antibacterial activity of biosynthesized Ag NPs

Gram-negative bacteria [45]. All this aforementioned evidence suggests the potential antibacterial activity of Ag NPs against Gram-positive and Gram-negative bacteria, with a great emphasis on Gram-positive bacteria. These results possibly open new avenues for therapeutic potential against antibiotic-resistant bacteria. Ag NPs could frequently release silver ions (Ag^+), which might be considered one of the mechanisms behind the bactericidal activity of Ag NPs. The positively charged Ag^+ plays a vital role to exhibit the silver's antibacterial or toxicity activities of the silver (Ag), and to maintain its antibacterial or toxicity activities, the Ag should be in its ionized state. Due to the electrostatic attraction and affinity toward the sulfur proteins, the Ag^+ ions adheres to the cytoplasm and cell wall, significantly enhancing the permeability, leading to the disruptions of bacterial casings.

5 Conclusion

The present research work on the basis of bamboo leaves extract secondary metabolites biosynthesis of Ag NPs was carried out. The secondary metabolites responsible for the reduction and capping agent of Ag NPs are present in the bamboo leaves extract. XRD analysis confirmed the formation of Ag NPs and was well matched with the standard card number. The UV–Vis spectroscopy determined the absorption peak at 425 nm; FTIR analysis indicated the presence of the various functional groups in the Ag NPs. The morphology of particle stability, average particle size, shape of the particles were analyzed by FESEM, DLS, and TEM. The bamboo-mediated Ag NPs showed potent antibacterial activity against microbial pathogens. The synthesized Ag NPs suggested significant scavenging activity by reducing DPPH free radicals. The bamboo-mediated Ag NPs resulted in dose-dependent anticancer against MCF-7 breast cancer cell lines showing good cell viability at various concentrations. This complete study concludes that bamboo leaves extract-mediated Ag NPs have excellent antibacterial, antioxidant, and anticancer activity. This approach of synthesized Ag NPs can be a used potential application in biomedical, and it may also be used in face mask coatings to prevent the coronavirus in the future due to being eco-friendly, cheap, non-toxic, and strong effective against pathogens. Finally, synthesized Ag NPs have been employed successfully to degrade the organic contaminant methylene blue.

Acknowledgements Authors acknowledge the financial support from Maharashtra Bamboo Development Board (MBDB), Nagpur (Grant No: MD/MBDB/CR-86/18-19/589). The authors also sincerely acknowledge the encouragement given by Sri T. Sai Kumar Reddy, MD, MBDB, Nagpur, to carry out this work.

Author contributions NJ investigation, data curation, writing—original draft, methodology, analysis, AA investigation, data curation, NA: formal analysis, TVR conceptualization, supervision, formal analysis, writing—review and editing, SV resources, formal analysis.

Data availability All data that support the findings of this study are included in the article.

Declarations

Conflict of interest The authors declare that they have no conflict of interest.

References

1. N. Tehri, A. Vashishth, A. Gahlaut, V. Hooda, Inorg. Nano-Metal Chem. **52**, 1 (2022)
2. S. Ahmed, M. Ahmad, B.L. Swami, S. Ikram, J. Adv. Res. **7**, 17 (2016)
3. M. Rafique, I. Sadaf, M.S. Rafique, M.B. Tahir, Artif. Cells, Nanomedicine Biotechnol. **45**, 1272 (2017)
4. M. Rai, A.P. Ingle, S. Birla, A. Yadav, C.A. Dos Santos, Crit. Rev. Microbiol. **42**, 696 (2016)
5. X.F. Zhang, F.H. Huang, G.L. Zhang, D.P. Bai, M. de Felici, Y.F. Huang, S. Gurunathan, Int. J. Nanomedicine **12**, 7551 (2017)
6. X.F. Zhang, Z.G. Liu, W. Shen, S. Gurunathan, Int. J. Mol. Sci. **17**(9), 1534 (2016)
7. S. Scandorieiro, L.C. de Camargo, C.A.C. Lancheros, S.F. Yamada-Ogatta, C.V. Nakamura, A.G. de Oliveira, C.G.T.J. Andrade, N. Duran, G. Nakazato, R.K.T. Kobayashi, Front. Microbiol. **7**, 1 (2016)
8. M. Kim, S. Ozone, T. Kim, H. Higashi, T. Seto, KONA Powder Part. J. **2017**, 80 (2017)
9. H.A. Widatalla, L.F. Yassin, A.A. Alrasheid, S.A.R. Ahmed, M.O. Widdatallah, S.H. Eltilib, A.A. Mohamed, Nanoscale Adv. **44**, 911 (2022)
10. M. Govarthanan, Y.S. Seo, K.J. Lee, I.B. Jung, H.J. Ju, J.S. Kim, M. Cho, S. Kamala-Kannan, B.T. Oh, Artif. Cells, Nanomedicine Biotechnol. **44**, 1878 (2016)
11. G. Marslin, K. Siram, Q. Maqbool, R.K. Selvakesavan, D. Kruszka, P. Kachlicki, G. Franklin, Materials (Basel). **11**, 1 (2018)
12 J.M. Jacob, R. Ravindran, M. Narayanan, S.M. Samuel, A. Pugazhendhi, G. Kumar, Curr. Opin. Environ. Sci. Heal. **20**, 100163 (2021)
13. P. Velmurugan, S.C. Hong, A. Aravinthan, S.H. Jang, P.I. Yi, Y.C. Song, E.S. Jung, J.S. Park, S. Sivakumar, Arab. J. Sci. Eng. **42**, 201 (2017)
14 M. Velu, J.H. Lee, W.S. Chang, N. Lovanh, Y.J. Park, P. Jayanthi, V. Palanivel, B.T. Oh, Biotech **7**, 1 (2017)
15. B.A. Zsembik, Handb. Fam. Heal. Interdiscip. Perspect. **6**, 40 (2006)
16. R. Sankar, P. Manikandan, V. Malarvizhi, T. Fathima, K.S. Shivashangari, V. Ravikumar, Spectrochim. Acta-Part A Mol. Biomol. Spectrosc. **121**, 746 (2014)
17. S. Ahmed, M. Ahmad, B.L. Swami, S. Ikram, J. Radiat. Res. Appl. Sci. **9**, 111 (2016)
18. H.M.M. Ibrahim, J. Radiat. Res. Appl. Sci. **8**, 265 (2015)
19. M.M.H. Khalil, E.H. Ismail, K.Z. El-Baghdady, D. Mohamed, Arab. J. Chem. **7**, 1131 (2014)
20. N. Kumar, K. Biswas, R.K. Gupta, RSC Adv. **6**, 111380 (2016)
21. K. Parveen, V. Banse, L. Ledwani, AIP Conf. Proc. **11**, 1724 (2016)

22 V. Soni, A.K. Jha, J. Dwivedi, P. Soni, Tang Humanitas Med. **3**, 201–203 (2013)
23. G.Y. Coffie, C. Antwi-Boasiako, N.A. Darkwa, J. Pharmacogn. Phytochem. **2**, 34 (2014)
24. A. Tanaka, Q. Zhu, H. Tan, H. Horiba, K. Ohnuki, Y. Mori, R. Yamauchi, H. Ishikawa, A. Iwamoto, H. Kawahara, K. Shimizu, Molecules **19**, 8238 (2014)
25. P. Phytochemical, A. Of, Molicule. **05**, 1341 (2018)
26 A.C. Iwansyah, R. Kumalasari, D.A. Darmajana, L. Ratnawati, IOP Conf. Ser. Earth Environ. Sci. **251**, 12017 (2019)
27. P.E. Das, I.A. Abu-Yousef, A.F. Majdalawieh, S. Narasimhan, P. Poltronieri, Molecules **25**, E555 (2020)
28. C. Senthilkumar, S.A.V. Anbazhagana, J. Mol. Struct. **1263**, 133139 (2022)
29. Z. Gharari, P. Hanachi, T.R. Walker, Anal. Biochem. **653**, 114786 (2022)
30. X. Hu, L. Wu, M. Du, L. Wang, Arab. J. Chem. **15**, 103763 (2022)
31 Y. Reyes-Vidal, R. Suarez-Rojas, C. Ruiz, J. Torres, S. Tefan, T. Alu, A. Méndez, G. Trejo, Appl Surf Sci. **342**, 34–41 (2015)
32. G. Ali, A. Khan, A. Shahzad, A. Alhodaib, M. Qasim, I. Naz, A. Rehman, Arab. J. Chem. **15**, 104053 (2022)
33. I. Ullah, K. Tahir, A.U. Khan, K. Albalawi, B. Li, A.A. El-Zahhar, V. Jevtovic, H.S. Al-Shehri, B.H. Asghar, M.M. Alghamdi, Inorg. Chem. Commun. **141**, 109539 (2022)
34. A. Sahin Yaglioglu, R. Erenler, E.N. Gecer, N. Genc, J. Inorg. Organomet. Polym. Mater. **11**, 123–432 (2022)
35. L. Farhadi, M. Mohtashami, J. Saeidi, M. Azimi-nezhad, G. Taheri, R. Khojasteh-Taheri, A. Rezagholizade-Shirvan, E. Shamloo, A. Ghasemi, J. Inorg. Organomet. Polym. Mater. **32**, 1637 (2022)
36. G. Premanand, N. Shanmugam, N. Kannadasan, K. Sathishkumar, G. Viruthagiri, Appl. Nanosci. **6**, 409 (2016)
37 B. Ajitha, Y.A.K. Reddy, P.S. Reddy, Mater. Sci. Eng. C **49**, 373 (2015)
38 R. Rajasekar, R. Thanasamy, M. Samuel, T.N.J.I. Edison, N. Raman, Biochem. Eng. J. **187**, 108447 (2022)
39. S. Subramaniam, S. Kumarasamy, M. Narayanan, M. Ranganathan, T. Rathinavel, A. Chinnathambi, T.A. Alahmadi, I. Karuppusamy, A. Pugazhendhi, K. Whangchai, Environ. Res. **204**, 111987 (2022)
40 M. Silva-Ichantea, Y. Reyes-Vidala, F. Javier, B. Valenzuelaa, J.C. Ballesterosd, E. Arcigaa, Ş Ţăluc, A. Méndez-Alboresb, G. Trejo, J Electroanal Chem. **823**, 328–334 (2018)
41. D. Das, B.C. Nath, P. Phukon, S.K. Dolci, ColloidsSurf B Biointerfaces **101**, 430–433 (2013)
42 M.A. Aza, Z. Kanwal, A. Rauf, A.N. Sabri, S. Raza, S. Naseem, Nanomaterials **6**, 1–5 (2016)
43. S. Pirtarighat, M. Ghannadnia, S. Baghshahi, Mater Sci Eng C **98**, 250–255 (2019)
44 A. Mendez-Albores, S.G. Gonzalez-Arellano, Y. Reyes-Vidal, J. Torres, S. Tefan, T. Alu, B. Cercado, G. Trejo, J Alloy Comp. **710**, 302–311 (2017)
45 M.M.N. El-Dein, Z.A. Baka, A. Dobara, M.I. El-Sayed, A.K. El-Sayed, M.M. El-Zahid, J microbiol. **10**(4), 648–656 (2021)